Study of Moist Air Flow Through the Ludwieg Tube

Seung-Cheol Baek, Soon-Bum Kwon
Department of Mechanical Engineering, Kyungpook National University 1370, Sankyuk-dong, Daegu 702-701, Korea
Heuy-Dong Kim*
School of Mechanical Engineering, Andong National University, Songchun-dong, Andong 760-749, Korea
Toshiaki Setoguchi, Sigeru Matsuo
Department of Mechanical Engineering, Saga University, Honjo-machi, Saga-shi, Saga 840-8502, Japan
Raghu S. Raghunathan
School of Aeronautical Engineering, The Queen's University of Belfast, David Keir Building, Stranmillis Road, Belfast BT9 5AG, Northern Ireland, UK

The time-dependent behavior of unsteady condensation of moist air through the Ludwieg tube is investigated by using a computational fluid dynamics (CFD) work. The two-dimensional, compressible, Navier-Stokes equations, fully coupled with the condensate droplet growth equations, are numerically solved by a third-order MUSCL type TVD finite-difference scheme, with a second-order fractional time step. Baldwin-Lomax turbulence model is employed to close the governing equations. The predicted results are compared with the previous experiments using the Ludwieg tube with a diaphragm downstream. The present computations represent the experimental flows well. The time-dependent unsteady condensation characteristics are discussed based upon the present predicted results. The results obtained clearly show that for an initial relative humidity below 30% there is no periodic oscillation of the condensation shock wave, but for an initial relative humidity over 40% the periodic excursions of the condensation shock occurs in the Ludwieg tube, and the frequency increases with the initial relative humidity. It is also found that total pressure loss due to unsteady condensation in the Ludwieg tube should not be ignored even for a very low initial relative humidity and it results from the periodic excursions of the condensation shock wave.

Key Words: Ludwieg Tube, Compressible Flow, Condensation Shock Wave, Periodic Flow, Non-Equilibrium Condensation, Supersonic Nozzle

Nomenclature

a : Speed of sound
C_p : Specific heat at constant pressure [J/(kg·K)]
E_S : Total energy per unit volume [J/m^3]
E, F: Numerical flux
g : Condensate mass fraction [-]
h : Tube height [mm]
h^* : Characteristic length [mm]
I : Nucleation rate [1/(m^3·s)]
J : Jacobian
k : Boltzmann constant [J/K]
L : Latent heat [J/kg]
M : Molecular weight [kg/kmol]
m : Mass [kg]
Pr : Prandtl number

* Corresponding Author,
E-mail : kimhd@andong.ac.kr
TEL : +82-54-820-5622; **FAX** : +82-54-823-5495
School of Mechanical Engineering, Andong National University, Songchun-dong, Andong 760-749, Korea
(Manuscript **Received** March 2, 2002; **Revised** September 27, 2003)

p : Pressure [Pa]
p_∞ : Flat film equilibrium vapour pressure [Pa]
Q : Source term
R, S : Viscous term
Re : Reynolds number [-]
$\Re$: Gas constant [J/(kg·K)]
r : Droplet radius [m]
r_c : Critical droplet radius [m]
S : Initial degree of supersaturation [-]
t : Time [s] or temperature [℃]
T : Temperature [K]
U : Conservation term
u, v : Cartesian velocity components [m/s]
x, y : Cartesian coordinates [m]
γ : Ratio of specific heats [-]
Γ : Accomodation coefficient of nucleation [-]
ζ : Coefficient of surface tension [-]
μ : Dynamic viscosity [Pa·s]
κ : Bulk viscosity
λ : Coefficient of second viscosity
ξ, η : Generalized coordinates [-]
ξ : Condensation coefficient [-] λ
ρ : Density [kg/m^3]
σ : Surface tension [N/m]
σ_∞ : Surface tension of an infinite flat-film [-]

Sub/superscripts

0 : Stagnation state
∞ : Plane surface
l : Liquid or laminar state
m : Mixture
r : Droplet radius
v : Vapour
s : Saturation
t : Turbulent state
- : Dimensional quantity
* : Nondimensional quantity

1. Introduction

A supersonic flow with heat addition has received considerable attention for last 40 years. Typical example of such flow phenomena is often found in Laval nozzle flows with the unsteady condensation of moist air or steam (Wegener and Mack, 1958 ; Frank, 1985), which is rapidly expanded through the nozzle. In general, the process of heat addition can lead to unsteady wave motions even in a supersonic flow field. Some kinds of flow instabilities are produced in the nozzle, as the release of the latent heat of the condensation exceeds a critical value (Wegener, 1970 ; Wegener and Wu, 1977). The flow instabilities are closely associated with condensation shock motions in the nozzle.

Depending on the nozzle supply conditions, it has been well known that the flow instabilities have three different types of the condensation shock wave motions (Wegener and Cagliostro, 1973 ; Matsuo et al., 1985) 1) Mode A oscillation : a condensation shock builds up periodically in the divergent part of nozzle and moves upstream the nozzle throat. 2) Mode B oscillation : a condensation shock builds up periodically in the divergent part of nozzle, moving upstream but it dies out before it reaches the nozzle throat. 3) Mode C oscillation : No periodic condensation shock motions build up but the condensation shock oscillates around a certain time-mean location in the divergent part of nozzle. These instabilities usually cause noise and vibration problems of flow device. Detailed understanding and prediction of such a flow are of practical importance for various engineering applications. Although much previous work (Wegener and Cagliostro, 1973 ; Matsuo et al., 1985 ; Adam and Schnerr, 1997 ; Setoguchi et al., 2001a) showed substantial progress in understanding the complex periodic behavior of the nozzle flows caused by the unsteady condensation, many microscopic problems with regard to the unsteady condensation still remain unanswered ; time-dependent condensation physics and the related energy losses are not yet fully known.

A short duration supersonic wind tunnel, called a Ludwieg tube (or a Tube wind tunnel), has long been used to investigate the process of head addition of the condensation in the nozzle (Cagliostro, 1972 ; Matsuo et al., 1985), since it provided well controlled flow conditions that permit operation with increased initial relative humidities and pressures, as well as variable supply temperatures. Recently the Ludwieg tube is receiving a renewed interest in simulating a space

transportation system (Friehmelt et al., 1993; Cable and Cox, 1963), because it is easy to achieve high Mach number and Reynolds numbers with relatively low turbulence, compared with the conventional supersonic and hypersonic wind tunnels. However the short duration of steady flow makes the flow measurements in the Ludwieg tube extremely difficult.

According to the previous some experimental work, it has been known that unsteady condensation of moist air in the Ludwieg tube can lead to considerable total pressure losses and flow instabilities as well (Hill, 1966; Bull, 1952). Wegener & Cagliostro (1973) showed that the unstable flow in the Ludwieg tube was caused by the heat addition due to unsteady condensation of moist air. They also carried out a dimensional analysis to get insight into the flow mechanism associated with unsteady compressible flow with heat addition, and showed that the frequency of the unsteady flow was an increasing function of the supply relative and specific humidities, respectively. But they did not get an understanding of the details of the unsteady condensation process in the Ludwieg tube. Barschdorff & Fillipov (1970) and Zierep & Lin (1967) derived a similarity law to express the dimensionless frequency of the unsteady flow within certain ranges of nozzle geometries and supply conditions.

Matsuo et al.(1983) conducted some experiment using the Ludwieg tube with a downstream diaphragm and obtained a nondimensional frequency of the unsteady periodic flows with condensation shock wave in terms of the flow properties at supply conditions and nozzle configurations. However the moist air flow through the Ludwieg tube has been qualitatively characterized by only some optical visualization and wall pressure measurements at several points in the flow field. Thus detailed flow information with regard to time-dependent unsteady condensation in the Ludwieg tube is not yet well known, since experiment is hard to reveal it. For instance, how does the unsteady condensation influence the performance of the Ludwieg tube with a very short operation? Under the unsteady periodic flows, how is the time-dependent unsteady condensation varied in the Ludwieg tube? Is the prediction of the total pressure losses due to the time-dependent unsteady condensation possible? Further study is required to understand the detailed effects of the unsteady condensation on the Ludwieg tube flow.

A computational fluid dynamics (CFD) method may give help to properly simulate the unsteady flow in the Ludwieg tube. It not only models the gross pattern of the flow field, but also details such unsteady flow features that the experiments cannot readily disclose. None of the computational work to date has produced a clear description of the cyclic behavior in the Ludwieg tubes, and to the best of the authors' knowledge, applications of CFD technique to this field are very rare at present.

In the present study, a computational fluid dynamics (CFD) work is applied to predict the unsteady condensation phenomena and associated flow instabilities in the Ludwieg tube. The Ludwieg tube with a downstream diaphragm is simulated using the two-dimensional Navier-Stokes equations. In computations, a droplet growth equation is incorporated into the governing equations, which are numerically solved by a third-order MUSCL type TVD finite-difference scheme with a second-order fractional time step. Baldwin-Lomax turbulence model is employed to close the governing equations (Baldwin and Lomax, 1978). The predicted results are compared with the previous experiments (Matsuo et al., 1983) using the Ludwieg tube with a diaphragm downstream.

2. Computational Analysis

2.1 Brief description of the Ludwieg tube flow with a downstream diaphragm

The Ludwieg tube mainly consists of the high-pressure tube, supersonic nozzle, diaphragm (or quick opening value), and low-pressure tube. Once the diaphragm is ruptured, an expansion wave propagates back toward the high-pressure tube (at state ④ in Fig. 1) and at the same time, a shock wave propagates downstream toward the low-pressure tube (at state ①). Just behind the

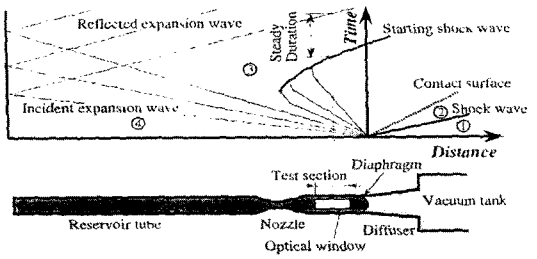

Fig. 1 Principle of the Ludwieg tube with a downstream diaphragm

tail of the expansion waves (at state ③), the flow properties such as pressure, temperature, density, are kept constant during a short duration. These properties are used as a supply condition, like a conventional supersonic wind tunnel system.

In general, there have been two-different types of Ludwieg tubes, depending on the location of the diaphragm: upstream diaphragm type Ludwieg tube and downstream diaphragm type Ludwieg tube. Figure 1 schematically shows the principle of the downstream diaphragm type Ludwieg tube. Due to the expansion waves propagating upstream after the diaphragm rupture, the flow is accelerated to a supersonic speed through the nozzle, and consequently leading a shock wave in the test section. The steady flow in the Ludwieg tube is kept until the expansion waves, which are reflected from the end wall of the high-pressure tube, come back to the test section, as shown in Fig. 1.

This steady duration is, in general, proportional to the length of the high-pressure tube, and inversely proportional to the speed of sound, which is obtained from the flow properties just behind the tail of the expansion waves (state ③). The decrease in density and temperature behind the tail of the expansion waves makes Reynolds number at the nozzle inlet considerably high, compared with the conventional supersonic wind tunnels. The downstream diaphragm type Ludwieg tube has several merits over the upstream diaphragm type; shock wave or contact surface does not directly influence the flow field in the test section, and low turbulence flow can be obtained in the test section. However it requires a longer time to start the steady flow in the test section, compared with the upstream diaphragm type. For more details the readers are referred to typical textbooks.

2.2 Governing equations

For simplicity of the present computational analysis, several assumptions are made; there is no velocity slip and no temperature difference between condensate particles and medium gas flows, and thus the energy relaxation processes between two phases are not considered in the present analysis. Due to very small condensate particles, the effect of the particles on pressure field of flow can be neglected. The resulting governing equations are the unsteady, two-dimensional, compressible, Navier-Stokes equations, which are given by Eq. (1) (Setoguchi et al., 2001a; Setoguchi et al., 2001b).

$$\frac{\partial Q}{\partial t}+\frac{\partial E}{\partial x}+\frac{\partial F}{\partial y}=\frac{1}{\mathrm{Re}}\left(\frac{\partial R}{\partial x}+\frac{\partial S}{\partial y}\right)+H \quad (1)$$

where

$$Q=\begin{bmatrix}\rho_m\\ \rho_m u\\ \rho_m v\\ \rho_m E_t\\ \rho_m g\\ \rho_m D_1\\ \rho_m D_2\\ \rho_m D_3\end{bmatrix},\ E=\begin{bmatrix}\rho_m u\\ \rho_m u^2+p\\ \rho_m uv\\ u(E_t+p)\\ \rho_m ug\\ \rho_m uD_1\\ \rho_m uD_2\\ \rho_m uD_3\end{bmatrix},\ F=\begin{bmatrix}\rho_m v\\ \rho_m v\\ \rho_m v^2+p\\ v(E_t+p)\\ \rho_m vg\\ \rho_m vD_1\\ \rho_m vD_2\\ \rho_m vD_3\end{bmatrix},$$

$$R=\begin{bmatrix}0\\ \tau_{xx}\\ \tau_{xy}\\ \alpha\\ 0\\ 0\\ 0\\ 0\end{bmatrix},\ S=\begin{bmatrix}0\\ \tau_{yx}\\ \tau_{yy}\\ \alpha\\ 0\\ 0\\ 0\\ 0\end{bmatrix},\ H=\begin{bmatrix}0\\ 0\\ 0\\ 0\\ \rho_m\dot{g}\\ \rho_m\dot{D}_1\\ \rho_m\dot{D}_2\\ \rho_m\dot{D}_3\end{bmatrix} \quad (2)$$

In these equations.

$$E_t=\rho_m C_{P0}T-p+\frac{1}{2}\rho_m(u^2+v^2)-\rho_m gL \quad (3)$$

$$\alpha=u\tau_{xx}+v\tau_{yx}+\frac{\mu}{(\gamma-1)\mathrm{Pr}}\frac{\partial T}{\partial x} \quad (4)$$

$$\beta=u\tau_{xy}+v\tau_{yy}+\frac{\mu}{(\gamma-1)\mathrm{Pr}}\frac{\partial T}{\partial y} \quad (5)$$

$$p=G\left[E_t-\frac{1}{2}\rho_m(u^2+v^2)+\rho_m gL\right] \quad (6)$$

$$G=\left\{1-g\frac{M_m}{M_v}\right\}\Big/\left\{\frac{1}{\gamma-1}+g\frac{M_m}{M_v}\right\} \quad (7)$$

$$L=2.353\times10^6-5.72\times10^4(\ln p-10) -4.60\times10^3(\ln p-10)^2 \ (J/kg) \quad (8)$$

τ_{xx}, τ_{xy}, τ_{yx} and τ_{yy} above are components of viscous shear stresses. g(=$(m_l/(m_a+m_v+m_l))$ is condensate mass fraction. Subscript m refers to the mixture. g, D_1, D_2, and D_3 are given as follows ;

$$\dot{g}=\frac{dg}{dt}=\frac{\rho_l}{\rho_m}\frac{4\pi}{3}\left(r_c^3 I+\rho_m D_1\frac{\partial r}{\partial t}\right) \quad (9)$$

$$\dot{D}_1=\frac{dD_1}{dt}=\frac{4\pi r_c^2 I}{\rho_m}+D_2\frac{dr}{dt} \quad (10)$$

$$\dot{D}_2=\frac{dD_2}{dt}=\frac{8\pi r_c^2 I}{\rho_m}+D_3\frac{dr}{dt} \quad (11)$$

$$\dot{D}_3=\frac{dD_3}{dt}=\frac{8\pi I}{\rho_m} \quad (12)$$

The rate of formation of condensation droplet embryos per unit mass of mixture I, the critical radius of the condensation nuclei r_c and the radius growth rate are obtained from the classical theories of homogeneous condensation as

$$I_F=\Gamma\cdot I \quad (13)$$

$$I=\frac{1}{\rho_l}\left(\frac{p_v}{kT}\right)^2\sqrt{\frac{2\sigma M_v}{N_A\pi}}\exp\left\{\frac{-4\pi\sigma r_c^2}{3kT}\right\} \quad (14)$$

$$r_c=\frac{2\sigma}{\rho_l\Re T\ln(p_l/p_\infty)} \quad (15)$$

$$\dot{r}=\frac{dr}{dt}=\frac{\xi_c}{\rho_l}\frac{p_\infty}{\sqrt{2\pi\Re T}}\left(\frac{p_v}{p_\infty}-1\right) \quad (16)$$

$$p_\infty=10^{(-A/T+B)}\times101325(\mathrm{Pa}) \quad (17)$$

In Eq. (13) an accommodation coefficient, Γ is assumed to be unity in the present computations and in Eq. (17), A and B are constants depending on the medium gas temperature which are defined next :

$A=2263$, $B=6.064$ for $T=273\sim395$K,
$A=2672$, $B=7.582$ for $T=175\sim273$K

In the equations above, M, $\Re$, k, p_∞ are molecular weight, gas constant, Boltzmann constant and flat film equilibrium vapour pressure, respectively. Subscripts v and l refer to vapour and liquid phases, respectively. In Eq. (15), ξ_c is a condensation coefficient. Surface tension σ is given using the surface tension of an infinite flat-film σ_∞ and the coefficient of surface tension ζ.

$$\sigma=\zeta\sigma_\infty \quad (18)$$

$$\sigma_\infty=(128-0.192T)\times10^{-3}(\mathrm{N/m}) \quad (19)$$

In computations, the values chosen for ξ_c and ζ are assumed to be 0.1 and 1.22, respectively (Adam and Schnerr, 1997). Baldwin-Lomax model (Baldwin and Lomax, 1978) is employed to solve turbulence stresses. A third-order TVD (total variation diminishing) finite difference scheme with MUSCL (Yee, 1989) is used to discretize the spatial derivatives of the governing equations and a second-order central difference scheme is applied to the viscous terms. A second-order fractional time step is employed for the time integration.

The governing equation systems above are mapped from the physical plane (x, y) into a computational plane (ξ, η) of a general transform.

$$\frac{\partial\hat{Q}}{\partial t}+\frac{\partial\hat{E}}{\partial\xi}+\frac{\partial\hat{F}}{\partial\eta}=\frac{1}{\mathrm{Re}}\left(\frac{\partial\hat{R}}{\partial\xi}+\frac{\partial\hat{S}}{\partial\eta}\right)+\hat{H} \quad (20)$$

$$\hat{Q}=JQ,\ \hat{E}=J(\xi_x E+\xi_y F),\ \hat{F}=J(\eta_x E+\eta_y F)$$
$$\hat{R}=J(\xi_x R+\xi_y S),\ \hat{S}=J(\eta_x R+\eta_y S) \quad (21)$$
$$J^{-1}=|\,x_\xi y_\eta-y_\xi x_\eta\,|$$

The governing equations are non-dimensionalized using the reference values at the inlet conditions upstream of the nozzle, as next ;

$$u^*=\bar{u}/\bar{u}_o,\ v^*=\bar{v}/\bar{u}_o,\ x^*=\bar{x}/\bar{L},\ y^*=\bar{y}/\bar{L}$$
$$t^*=\bar{t}/(\bar{L}/\bar{u}_o),\ \rho^*=\bar{\rho}/\bar{\rho}_o,\ T^*=\bar{T}/\bar{T}_o,\ p^*=\bar{p}/(\bar{\rho}_o\bar{u}_o^2)=\bar{p}/k\bar{p}_o \quad (22)$$
$$\mu^*=\bar{\mu}/\bar{\mu}_o,\ k^*=\bar{k}/\bar{\mu}_o,\ e^*=\bar{e}/\bar{u}_o^2,\ E_s^*=E_s/(\bar{\rho}_o\bar{u}_o^2),\ a^*=\bar{a}/\bar{u}_o$$

To close the governing equations above, Baldwin-Lomax model is employed in computations. A third-order TVD (total variation diminishing) finite difference scheme with MUSCL (Setoguchi et al., 2001a ; Yee, 1989) is used to discretize the spatial derivatives, and a second order-central difference scheme for the viscous terms. A second-order upwind TVD scheme is applied to the droplet growth equation (Setoguchi et al., 2001a ; Setoguchi, 2001b), and a second order fractional step is employed for time integration.

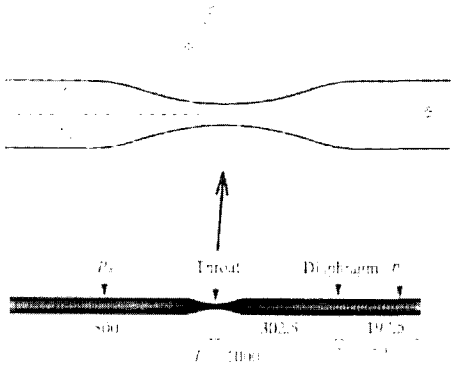

Fig. 2 Ludwieg tube flow for computation

2.3 Initial and boundary conditions

The Ludwieg tube for the present computational analysis is schematically shown in Fig. 2, which was also used for the previous experimental work by Matsuo et al.(1983) The Ludwieg tube consists of the upstream high-pressure tube, the convergent-divergent nozzle, and the downstream low-pressure tube. The Ludwieg tube has a length of 1000 mm. A diaphragm downstream of the nozzle throat locates at the low-pressure tube, being an origin (x=0) in the present computations and separates the high and low-pressure tubes. The high and low-pressure tubes have the same height of h=38 mm. The convergent-divergent nozzle with a throat height of h^* (=12 mm) is located at x=302.5 mm upstream of the diaphragm and is of a circular arc with its curvature radius of R^*=155 mm.

The pressures in the high and low-pressure tubes are defined as p_4 and p_1, respectively (see Fig. 1). In the present study, p_4 is kept constant at 101.3 kPa, but the ratio of $p_4/p_1(=p_{41})$ is varied between 3.0 and 5.0. The initial flow conditions in the high-pressure tube are given by, pressure p_4, relative humidity ϕ_4, temperature T_4, etc. In the present computations, T_4 is kept constant at 303 K, being the same to the temperature T_1 in the low-pressure tube. The initial relative humidity ϕ_4 is varied between 0% and 90%. According to the gasdynamics theory (Matsuo et al., 1983), these values correspond to the relative humidity ϕ_{03} of 0% and 221%, respectively, just behind the tail of the unsteady expansion waves (see Fig. 1).

The height h^* of the nozzle throat is yielded as a characteristic length scale in the present analysis. Moist air is used as a working fluid and assumed to be thermally and calorically perfect. To obtain different condensation shock waves in the nozzle, the initial relative humidity ϕ_4 is changed at fixed p_{41}. Inlet and outlet boundaries are constrained to the free boundary conditions. No-slip wall velocity is assumed on adiabatic wall condition of no heat transfer. Further, condensate mass fraction g=0 is given at the solid walls and the symmetry condition on the nozzle centerline.

The fineness of computational grid was examined to assure that the obtained solutions were independent of the grid employed. The resulting grids were 601×301 for the Ludwieg tube flow field, as shown in Fig. 2. The grids are clustered in the nozzle and wall boundary layers, so that computations provide more reasonable predictions. A solution convergence was obtained when the residuals for each of the conserved variables have reduced below the order of a magnitude 4. Another convergence criterion is to directly check the conserved quantities through the computational boundaries. The net mass flux was investigated if there were an applicable imbalance through the computational boundaries.

3. Results and Discussion

The present computations are compared with the previous experiment (Matsuo et al., 1983) of Ludwieg tube, as shown in Fig. 3. Both the experiments and computations are nearly the same conditions of p_{41}=3.0, ϕ_4=42% and T_4=302 K (=T_1), and show the condensation shock motions at each instant during a cycle of the periodic condensation shock oscillation. In all of the Schlieren pictures, note that the flow is supersonic just downstream of the nozzle throat. At t=0 μs, a starting shock wave denoted by "S" is found downstream of the nozzle throat and it interacts with the wall boundary layers, leading to a very complicated wave structure. Two condensation shock waves, denoted by "A" and "B", respec-

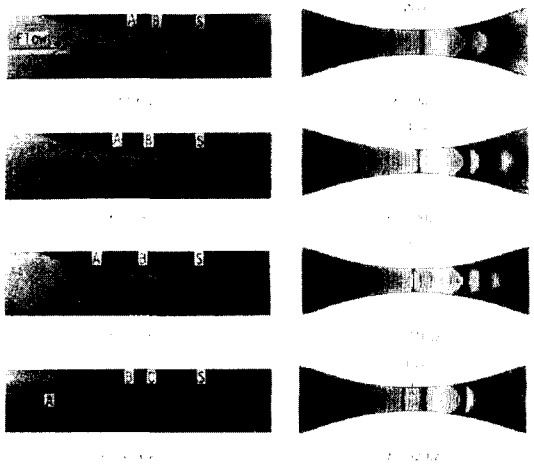

Fig. 3 Comparison between measured and predicted flow field

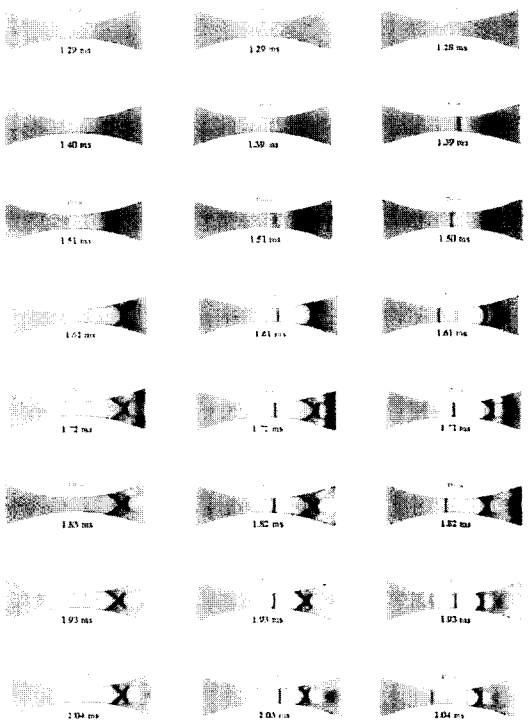

(a) ϕ_4=0% (b) ϕ_4=30% (c) ϕ_4=60%

Fig. 4 Predicted Schlieren images

tively, are found upstream and downstream of the nozzle throat. With time the condensation shock wave "A" moves upstream and its magnitude seems to be weaker due to the effect of the increase in the flow area. A new condensation shock wave appears behind the condensation shock wave "B", as the condensation shock wave "A" moves far upstream, as seen at t=350 μs. At the vicinity of the nozzle throat, the flow pattern is nearly the same to that at t=0 μs. From this measured result, it is found that the frequency of the unsteady motion of the condensation shock wave is about f=2.86 kHz.

The present computations show the qualitatively same trend to the experiments; the condensation shock motions with time and the starting shock structure are nearly the same. In considering such a highly complicated flow as the unsteady condensation and shock wave occurring in the Ludwieg tube, the agreement between both the results seems to be quite good, although the predicted frequency of the condensation shock motion is somewhat higher than the measured one. This ensures the validity of the present computations.

Figure 4(a, b and c) shows the predicted Schlieren images of the Ludwieg tube flow for ϕ_4=0% (dry air), 30% and 60%, respectively. The flow is started by the unsteady expansion wave propagating upstream just after the diaphragm rupture. A transient flow occurs inside the nozzle until an adiabatic starting shock wave occurs in the divergent part of the nozzle. At t=1.72 ms, it seems that the flow is fully developed inside the nozzle, and the adiabatic starting shock wave interacts with the wall boundary layers, leading to a lambda type shock wave. The boundary layers separate at the foot of the front leg of the lambda shock wave. For the dry air of ϕ_4=0%, there is no condensation shock wave, and the adiabatic shock wave does not significantly oscillate although the shock structures seem to be a little changed with time.

For ϕ_4=30%, the condensation shock wave occurs in the region between the nozzle throat and the location of the adiabatic shock wave. At t=1.51 ms, a certain weak disturbance, being the incipient condensation shock wave, appears downstream of the nozzle throat, and then a normal condensation shock is formed at t=1.72 ms. It does not appreciably oscillate with time. However it is found that the detailed structure and location

of the adiabatic shock wave is somewhat varied with time. For ϕ_4=60% the periodic motion of the condensation shock is seen in Fig. 4(c). At t=1.39 ms, the weak condensation shock wave appears a little downstream of the nozzle throat and moves upstream with time. The condensation shock wave decays as it passes beyond the nozzle throat, and consequently disappears far upstream of the nozzle throat. A new condensation shock wave occurs a little downstream of the nozzle throat, thus completing a cycle of the periodic motion. The frequency is found to be about 6 kHz. It is very likely that the periodic motion of the condensation shock wave influences the adiabatic shock location and structure.

At the each location along the center-line of the Ludwieg tube, the predicted static pressure variations with time are shown in Fig. 5 (see the points **t**, **a**, **b**, and **c**). The solid and dashed lines are the static pressure values for ϕ_4=80% and 30%, respectively. The head and tail of the expansion wave propagating upstream, just after the diaphragm rupture, are also presented. The static pressure is kept constant at p_4 before the head of the expansion wave reaches the location **t** (the nozzle throat). It seems that the head and tail of the expansion wave reaches the nozzle throat at t=0.8 ms and 1.7 ms, respectively, after the diaphragm rupture (t=0 ms). For ϕ_4=80% the static pressure at the nozzle throat quite periodically oscillates around a time-mean value, which is about 0.53p_4. However for ϕ_4=30% the pressure oscillation does not occur at the nozzle throat, but the pressure value seems to be somewhat lower than the time-mean value of the pressure oscillation for ϕ_4=80%.

The pressure oscillations are still found at the points a and b, as shown in Fig. 5. These are due to the periodic excursions of the condensation shock wave. At the point c, locating at x/h^*=−55.2, the amplitude of the pressure oscillation seems to be very weak due to the attenuation of the condensation shock wave occurring during the upstream excursion. From a comparison between the predicted results for the two ϕ_4 values presented, it is found that behind the tail of the unsteady expansion wave the static pressure of

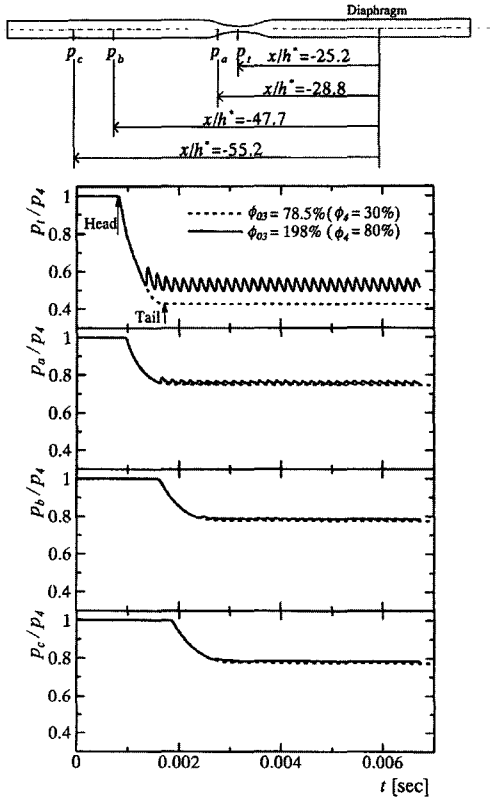

Fig. 5 Time histories of static pressures at several points on the center-line

ϕ_4=80% is somewhat higher than that of ϕ_4= 30%. This is due to the periodic excursion of the condensation shock wave.

For the effect of ϕ_4 on the periodic excursion of the condensation shock wave, Fig. 6 shows the static pressure variation with time at the nozzle throat. For the four different ϕ_4 presented, it seems that the pressure at the nozzle throat significantly changes depending on the initial relative humidity ϕ_4. For ϕ_4=30% the pressure behind the tail of the unsteady expansion wave does not oscillate with time, indicating no condensation shock excursion in the nozzle. With an increase in ϕ_4, a periodic oscillation in pressure is found, as indicated by the line **b**. Further increase in ϕ_4 makes the amplitude and frequency of the pressure oscillation higher (see the line **c**). For ϕ_4=80% it is known that the frequency of the pressure oscillation becomes higher but the amplitude is lower (see the line **d**), compared with

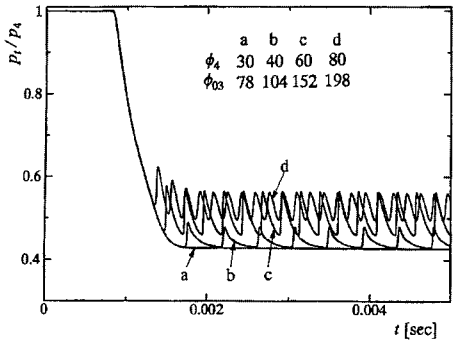

Fig. 6 Time histories of static pressures at nozzle throat

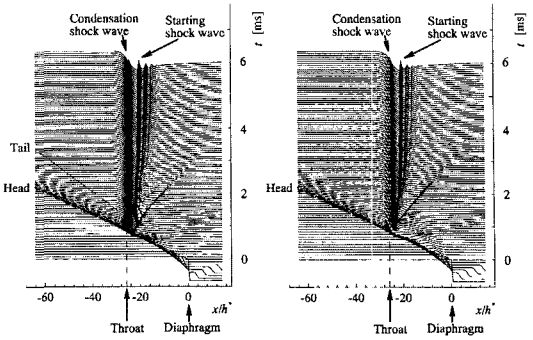

(a) ϕ_4=30%(ϕ_{03}=78.5%) (b) ϕ_4=80%(ϕ_{03}=198%)

Fig. 7 Wave diagram of the Ludwieg tube flow

that of ϕ_4=60%. This results from the fact that the higher the initial relative humidity ϕ_4 is, the closer is the condensation shock wave to the nozzle throat, consequently leading to the weaker condensation shock wave. From the results of Fig. 6, it is obvious that with a higher ϕ_4 the Ludwieg tube flow is highly unstable at the nozzle throat, even though the flow is supersonic just downstream of the nozzle throat.

In order to show the time-dependent behaviour of both the condensation shock and starting shock waves, Fig. 7(a and b) presents the x-t diagram for the static pressures along the center-line of the Ludwieg tube, where the head and tail of the unsteady expansion wave, condensation shock and starting shock are also shown. For ϕ_4=30% the weak condensation shock wave locates a little downstream of the nozzle throat, its location being independent of time. In this case, the pressure in the high-pressure tube is kept constant. The starting shock location also does not change with time. Downstream of the starting shock wave, some weak shocks result from the shock/boundary layer interaction. For ϕ_4=80% (see Fig. 7(b)), the pressure oscillations are still found far upstream of the nozzle throat. As described in Fig. 5, the periodic excursions of the condensation shock wave are responsible for the oscillation. Thus the Ludwieg tube flow with the moist air of a high relative humidity, even for an initial pressure ratio p_{41} enough to make the flow choke at the nozzle throat, would be changed with time.

In the present computations, for ϕ_4=35% the

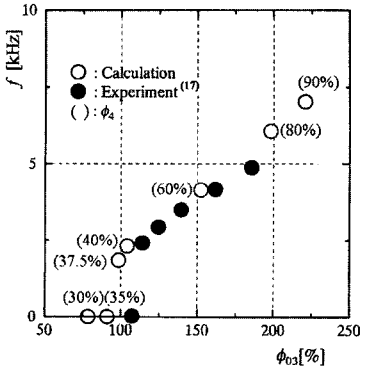

Fig. 8 Relationship between the periodic motions of condensation shock wave and initial relative humidity

unsteady excursion of the condensation shock wave was quite different from that for (ϕ=30 and 80%; the condensation shock wave, which occurred at a certain location in the divergent part of the nozzle, moved upstream with time but it died out before reaching the nozzle throat. Then a new condensation shock wave occurred at the nearly same location to the initial condensation shock wave, hence completing a cycle of the periodic motion. It is thus believed that the unsteady motion of the condensation shock wave for ϕ_4= 35% is a transitional process to such periodic motions as found for ϕ_4=60% and 80%.

Figure 8 shows the relationship between the frequency of the condensation shock wave oscillation and the relative humidity ϕ_{03}. The present predicted results are compared with the previous experiments (Matsuo et al., 1983). The relative humidity ϕ_{03} is calculated using a given ϕ_4, which

is also presented in the hollow circle in the Fig. 8. The present predicted results show that for a relative humidity ϕ_{03} lower than about 91%, there is no appreciable motion of the condensation shock wave, and for a relative humidity ϕ_{03} higher than 91% the frequency of the condensation shock motion increases with ϕ_{03}. Both the predicted and measured results are in a good agreement, although there is some difference in predicting the incipient relative humidity that the condensation shock wave starts to oscillate in the nozzle.

The time-dependent unsteady condensation characteristics are well shown in Fig. 9, where the static pressures **p**, nucleation rate **I** and condensate mass fraction **g** along the center-line of the Ludwieg tube are plotted in Fig. 9(a), (b) and (c), respectively. Here note that **I** is expressed by the number of condensate nuclei per unit time and unit volume, and **g** by the ratio of the condensate mass fraction to total mass flow through the Ludwieg tube. The arrow means the direction of the increasing time, each line indicating the time increment of about 110 μs.

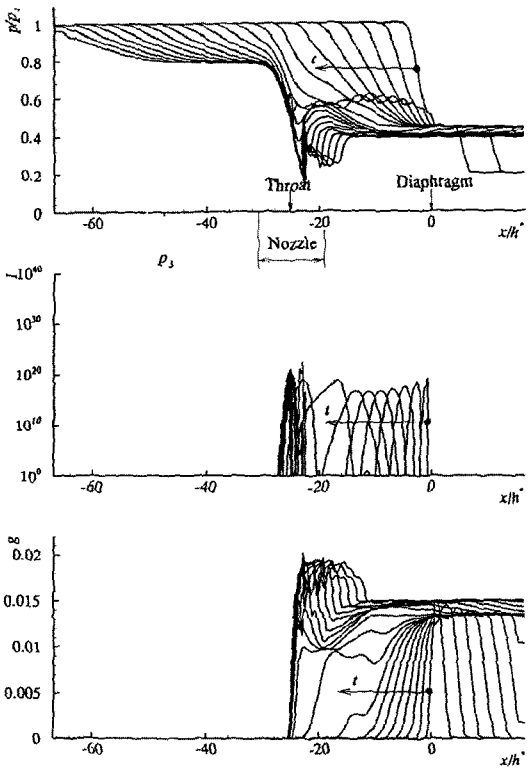

Fig. 9 Time-dependent behavior of unsteady condensation

It is found that the condensate nuclei start to occur just at the location of the diaphragm and move upstream with time, to the same direction to the propagation of the unsteady expansion wave. The spatial distribution of the condensate nucleus seems to be of a narrow zone with a sharp peak. The incipient point that the condensate mass fraction **g** starts to increase moves upstream with time. As the head of the unsteady expansion wave passes beyond the nozzle throat, the flow inside the nozzle is accelerated to a supersonic speed, leading to the condensation shock wave that oscillates with time. However it seems that the generation of the condensation nuclei is rather limited to a finite zone at the vicinity of the nozzle throat. The condensate nuclei are not found far upstream away from the nozzle throat, even when the unsteady expansion wave propagates there. It should be noted that the pressure behind the unsteady expansion wave is about $0.8p_4$, but it is about $0.6p_4$ for such a state that the unsteady condensation occurs downstream of the nozzle throat.

Additionally several computations were carried out to simulate a conventional shock tube flow with a constant area. In this case, the static pressure **p**, nucleation rate **I** and condensate mass fraction **g** were investigated at the same flow conditions to Fig. 9. The consequence was considerably different from that of the Ludwieg tube. The distributions of **I** and **g** moves far upstream with the unsteady expansion waves, still having any **I** and **g** distributions even at the region of $x/h^* < -30.0$, but Fig. 9 shows that those are limited to the region of $x/h^* >$ about -28.0. It is, thus, believed that in the Ludwieg tube with a downstream diaphragm, unsteady condensation does not occur far upstream of the nozzle throat, even when the expansion waves propagates to there.

The total pressure losses due to the unsteady condensation in the present Ludwieg tube are shown in Fig. 10(a) and (b), where p_{03} and p_{0c} mean the total pressures just behind the tail of the unsteady expansion wave and just upstream of the

starting shock wave, respectively. The error bar in the figure means the range of error produced in the repeated experiments. For an initial relative humidity ϕ_4 lower than about 40%, the total pressures are nearly identical to the values calculated by one-dimensional gasdynamics theory on dry air (see the dashed line) (Matsuo et al., 1983), but for an initial relative humidity ϕ_4 over 60%, the total pressures are deviated from the dashed line. This results from the pressure fluctuations due to the periodic upstream excursions of the condensation shock wave.

It is also found in Fig. 10(b) that p_{0c}/p_{03} considerably decreases with ϕ_4. According to the previous work using a conventional suction type wind tunnel, the total pressure loss due to unsteady condensation, even though it depends on the nozzle configuration and initial supply flow conditions, is estimated to be at best 5% (Matsuo et al., 1985; Kwon, 1986), even for a very high initial relative humidity. It is interesting to note that in the present Ludwieg tube, the total pressure loss amounts about 13%. Moreover, in the conventional suction type wind tunnel tests, a very low initial relative humidity ϕ_4, for instance, below 10%, is reasonably considered to be a dry air flow, since the unsteady condensation seldom occurs in the nozzle. But in the present Ludwieg tube, the total pressure loss for $\phi_4=10\%$ is estimated to be about 3%. Therefore the Ludwieg tube system using moist air as a test gas should be carefully designed even when it operates at the initial relative humidity conditions below $\phi_4=10\%$.

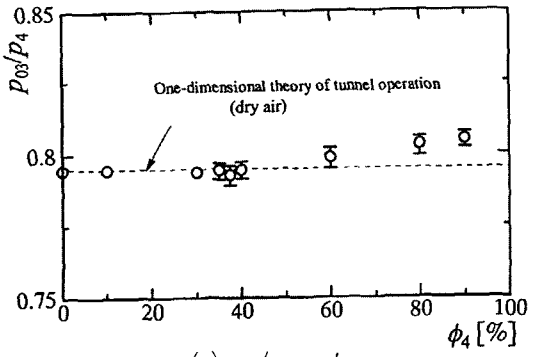

(a) p_{03}/p_4 vs ϕ_4

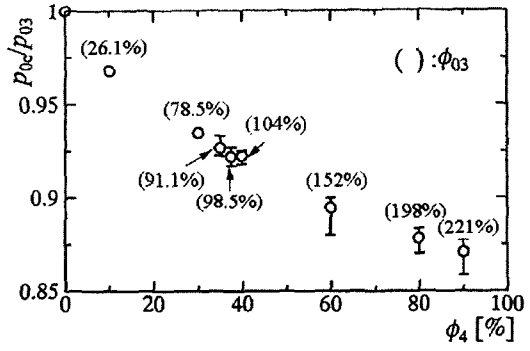

(b) p_{0c}/p_{03} vs ϕ_4

Fig. 10 Effect of the initial relative humidity on total pressure loss

4. Concluding Remarks

In order to investigate the time-dependent behavior of unsteady condensation of moist air through the Ludwieg tube, a computational fluid dynamics (CFD) work is applied to the two-dimensional, compressible, Navier-Stokes equations, fully coupled with the condensate droplet growth equations. A third-order MUSCL type TVD finite-difference scheme, with a second-order fractional time step, numerically solves the governing equations. Baldwin-Lomax turbulence model is employed to close the governing equations. The predicted results are compared with the previous experiments using the Ludwieg tube with a diaphragm downstream. It is found that for an initial relative humidity below 30% there is no periodic oscillation of the condensation shock wave, but for an initial relative humidity over 40% the periodic excursions of the condensation shock occurs in the Ludwieg tube, and the frequency increases with the initial relative humidity. For a high initial relative humidity the pressure oscillations occurs even far upstream of the nozzle throat in the Ludwieg tube. It is also found that total pressure loss due to unsteady condensation in the Ludwieg tube should not be ignored even for a very low initial relative humidity and it results from the periodic excursions of the condensation shock wave. The present computations clearly show the time-dependent behavior of the unsteady condensation of moist air, such as

nucleation rate, condensate mass fraction, condensation shock wave, unsteady condensation region.

References

Adam, S. and Schnerr, G. H., 1997, "Instabilities and Bifurcation of Non-Equilibrium Two-Phase Flows," *Journal Fluid Mechanics*, Vol. 348, pp. 1~28.

Baldwin, B. S. and Lomax, H., 1978, "Thin Layer Approximation and Algebraic Model for Separated Turbulent Flows," *AIAA paper* 78-257.

Barschdorff, D. and Fillipov, G. A., 1970, "Analysis of Certain Special Operating Modes of Laval Nozzles with Local Heat Supply," *Heat Transfer J.*, Vol. 2, No. 5, pp. 76~87.

Bull, G. V., 1952, "Investigation into the Operating Cycle of a Two-Dimensional Supersonic Wind Tunnel," *Journal of Aeronautical Sciences*, pp. 609~614.

Cable, A. J. and Cox, R. N., 1963, "The Ludwieg Pressure Tube Supersonic Wind Tunnel," *The Aeronautical Quarterly*, Vol. 14, No. 2, pp. 143~157.

Cagliostro, D. J., 1972, "Periodic Compressible Nozzle Flow caused by Heat Addition due to Condensation," Ph. D Thesis Yale University, New Haven.

Frank, W., 1985, "Condensation Phenomena in Supersonic Nozzles," *Acta Mechanica*, Vol. 54, pp. 135~156.

Friehmelt, H., Koppenwaller, G. and Muller-Eigner, R., 1993, "Calibration and First Results of a Redesigned Ludwieg Expansion Tube," AIAA Paper 93-5001.

Hill, P. G., 1966, "Condensation of Water Vapour during Supersonic Expansion in Nozzles," *Jour. Fluid Mechanics*, Vol. 25, No. 3, pp. 593~620.

Kwon, S. B., 1986, "The Study of Characteristics of Condensation Shock Waves," Ph. D. Thesis, Kyushu University, Japan.

Matsuo, K., Kawagoe, S., Sonoda, K. and Setoguchi, T., 1985a, "Oscillations of Laval Nozzle Flow with Condensation (part 2, on the mechanism of oscillations and their amplitudes)," *Bulletin of JSME*, Vol. 28, No. 235, pp. 88~93.

Matsuo, K., Kawagoe, S., Sonoda, K. and Sakao, K., 1985b, "Studies of Condensation Shock Waves (part 1, mechanism of their formation)," *Bulletin of JSME*, Vol. 28, No. 241, pp. 1416~1422.

Matsuo, K., Kawagoe, S., Sonoda, K. and Setoguchi, T., 1983, "Oscillations of Laval Nozzle Flow with Condensation (part 1, on the range of oscillations and their frequencies)," *JSME J.*, Vol. 26, No. 219, pp. 1556~1562.

Schnerr, G. H. and Dohrmann. U., 1990, "Transonic Flow around Airfoils with Relaxation and Energy Supply by Homogeneous Condensation," *AIAA J.*, Vol. 32, pp. 101~107.

Setoguchi, T., Matsuo, S. and Kim, H. D., 2001, "Passive Control of the Condensation Shock Wave Oscillations in a Transonic Nozzle," *Journal of Sound and Vibration* (to be published).

Setoguchi, T., Kim, H. D. and Matsuo, S., 2001, "Passive Control of the Condensation Shock Wave in a Transonic Nozzle," *Applied Scientific Research, International Journal on the Applications of Fluid Dynamics* (to be published).

Wegener P. P. and Mack, L. M., 1958, "Condensation in Supersonic Hypersonic Wind Tunnels," *Adv. in Applied Mechanics*, Vol. 5, pp. 307~447.

Wegener, P. P., 1970, "Nonequilibrium flows Part 2," Marcel Dekker Inc., pp. 163~242.

Wegener, P. P. and Wu, B., 1977, "Gasdynamics and Homogeneous Nucleation," *Nucleation Phenomena*, Vol. 7, pp. 325~402. Ed. by A. C. Zettlemoyer.

Wegener, P. P. and Cagliostro, D. J., 1973, "Periodic Nozzle Flow with Heat Addition," *Combustion Science and Technology*, Vol. 6, pp. 269~277.

Yee, H. C., 1989, "A Class of High-Resolution Explicit and Implicit Shock-Capturing Methods," NASA TM-89464.

Zierep, J. and Lin, S., 1967, "Bestimung des kondensationsbeginns kondensation bei entspannung feuchter luft in ueberschallduesen," Forsch. Ing.-Wes., Vol. 33, pp. 169~172.